# Four-level N-scheme crossover resonances in Rb saturation spectroscopy in magnetic fields

S. Scotto,[1,2] D. Ciampini,[2,3,4] C. Rizzo,[1] and E. Arimondo[1,2,3,4]

[1]*Laboratoire National des Champs Magntiques Intenses (UPR 3228, CNRS-UPS-UJF-INSA), 143 Avenue de Rangueil, 31400 Toulouse, France*

[2]*Dipartimento di Fisica "E. Fermi", Università di Pisa, Largo Bruno Pontecorvo 3, 56127 Pisa, Italy*

[3]*INO-CNR, Via G. Moruzzi 1, 56124 Pisa, Italy*

[4]*CNISM UdR, Dipartimento di Fisica "E. Fermi", Università di Pisa, Largo B. Pontecorvo 3, 56127 Pisa, Italy*

(Received 22 September 2015; published 7 December 2015)

We perform saturated absorption spectroscopy on the $D_2$ line for room temperature rubidium atoms immersed in magnetic fields within the 0.05–0.13 T range. At those medium-high field values the hyperfine structure in the excited state is broken by the Zeeman effect, while in the ground-state hyperfine structure and Zeeman shifts are comparable. The observed spectra are composed by a large number of absorption lines. We identify them as saturated absorptions on two-level systems, on three-level systems in a V configuration, and on four-level systems in an N or double-N configuration where two optical transitions not sharing a common level are coupled by spontaneous emission decays. We analyze the intensity of all those transitions within a unified simple theoretical model. We concentrate our attention on the double-N crossovers signals whose intensity is very large because of the symmetry in the branching ratios of the four levels. We point out that these structures, present in all alkali-metal atoms at medium-high magnetic fields, have interesting properties for electromagnetically induced transparency and slow light applications.

DOI: 10.1103/PhysRevA.92.063810 PACS number(s): 42.62.Fi, 32.60.+i, 32.30.Jc, 32.70.Fw

## I. INTRODUCTION

The laser action on atoms modifies the level occupation, and in addition may produce coherences associated with the quantum mechanical superposition of atomic states. The development of laser spectroscopy tools and the availability of samples with new features has allowed the exploration of a larger set of coherent and incoherent processes. Moving from two-level systems to three-level ones, phenomena such as coherent population trapping, electromagnetically induced transparency, and slow light were discovered and largely exploited [1]. This trend was confirmed by the search for the new properties of four-level schemes, forming the so-called N configuration, with the first proposition by Harris and Yamamoto [2], followed by the experimental investigation by several authors [3–6], with line shape contributions more recently explored by Abi-Salloum *et al.* [7].

Here we explore the high-resolution absorption spectra of rubidium atoms in medium-high magnetic fields. From a technical point of view the fields we explore around 0.1 T are low compared to the 100-T maximal fields produced at dedicated facilities. However in a standard laboratory the use of permanent magnets allow one to apply fields around 1 T at a short distance from the magnets. Our magnet assembly scheme allows the production of homogeneous magnetic fields over a large volume. From the atomic physics point of view the fields are classified from low to high by comparing the Zeeman splitting to the atomic structures, hyperfine and fine ones. Our exploration range corresponds to a hyperfine Paschen-Back regime for the optically excited state (high range), while for the ground state the Zeeman splitting and the hyperfine structure are comparable (medium range).

At low magnetic fields, i.e., in the presence of small Zeeman splittings of the atomic levels, the alkali-metal absorption spectra should be treated as multilevel systems, with a very complex interaction with the laser, typically eliminated by optical pumping into the extreme cycling transitions. This complexity is washed out at the 0.05–0.13 T magnetic fields of our investigation where the Zeeman effect breaks all degeneracies and a very large number of isolated and open two-level systems describe the laser-atom interaction. At those medium-high magnetic fields the hyperfine splitting is broken by the magnetic field in the excited state, but not in the ground state, and the usual optical dipole selection rules are broken by the magnetic field mixing. Therefore the spectra are characterized by several well-isolated three-level structures. In addition some peculiar, and very strong, features associated with different four-level N schemes are produced by the laser excitation. Similar strong absorption structures should appear in other alkali-metal spectra at those medium-high fields.

Sub-Doppler absorption signals produced by four-level systems, within an N configuration, were studied a long time ago, as soon the sub-Doppler saturated spectroscopy was introduced (see Refs. [8,9] and a review in Ref. [10]). Those studies were performed at magnetic fields lower than those of the present work, and therefore our features were not observed. Let us point out that in all our four-level schemes spontaneous emission coupling represents an intermediate step within the N structure. Therefore only a population transfer occurs, without creation of atomic coherences, unlike the coherent N schemes mentioned above triggered by the proposal of Harris and Yamamoto [2]. The large variety of four-level schemes associated with our intermediate magnetic field regime provides experimentalists with a flexible medium where different coherent processes can be implemented. At some magic magnetic field values and by replacing the spontaneous emission with stimulated emission (produced by close frequency additional lasers), our schemes may be converted into peculiar double-Λ structures.

Saturated absorption resonances in alkali-metal atom spectra in the presence of magnetic fields larger than 0.01 T

 

have been examined by several authors, also within the last few years (see, for instance, Refs. [11–16]). Because our study of the Zeeman effect in rubidium complements those works, our analysis includes the observation of absorption lines that are forbidden at zero magnetic field, but become allowed increasing the field due to the magnetic-field-induced mixing of the eigenstates. Our attention is focused on the strength of the saturated absorption signals associated with two-level schemes (TLS), V-scheme three-levels (VTL), and four-level N schemes. Our list does not include Λ three-level systems, because they are not present within the explored laser polarization schemes.

The theoretical description of saturation spectroscopy has a long history, with an early work by Hänsch [17] providing an introductory review. The standard approach is based on the steady-state solutions of the density matrix equations for the atomic levels excited by the control and probe lasers, as initiated in Ref. [18]. On the basis of that formalism Nakayama *et al.* [9,10] derived expressions for the signal intensities. The integration over the Doppler velocity distribution represents a key element for quantitative analysis, as in Refs. [19–22]. Our Zeeman spectra are composed of a large number of absorption lines, the exact number depending on the laser polarization scheme, and their largest majority is associated with two-level open systems, where the optical pumping into a dark state determines the signal intensity. The contribution of optical pumping into dark states is examined in Refs. [19,23]. We compare the relative amplitude of the absorption signals by using simple and universal formulas without performing a Doppler integration as required for precise amplitude determinations. The effect of transient optical pumping on the amplitude of the saturated absorption signal discussed in Refs. [19,24] is important for some experimental observations.

In Sec. II we rewrite the steady-state density matrix solution in a form appropriate to analyze open TLSs. The following Sec. III derives from that solution the intensities of the VTL and N absorption features. After a brief section presenting our apparatus, Sec. V discusses typical spectra and points out some observed forbidden lines. Section VI analyzes the intensity of all the measured absorption signals. A final section concludes our work including perspectives and applications of the present investigation.

## II. TWO-LEVEL OPEN SYSTEM

In order to compare the saturation absorption signals associated with a variety of optical transitions, for each given $|1\rangle \rightarrow |2\rangle$ TLS we introduce a theoretical relative line strength $f_{1-2}$ defined as the square of the dipole moment $D$ matrix element between initial and final states, normalized to the optical dipole matrix element for the strong cycling Zeeman transition of the $5\,^2S_{1/2} \rightarrow 5\,^2P_{3/2}$ $D_2$ line. Thus for a $^{87}$Rb transition we write

$$f_{1-2} = \frac{|\langle 1|D|2\rangle|^2}{|\langle 5\,^2S_{1/2}, F_g = 2, m_g = 2|D|5\,^2P_{3/2} F_e = 3, m_e = 3\rangle|^2}. \tag{1}$$

Therefore $f_{1-2}$ is equal to one for the cycling transition and smaller than one for all the open ones.

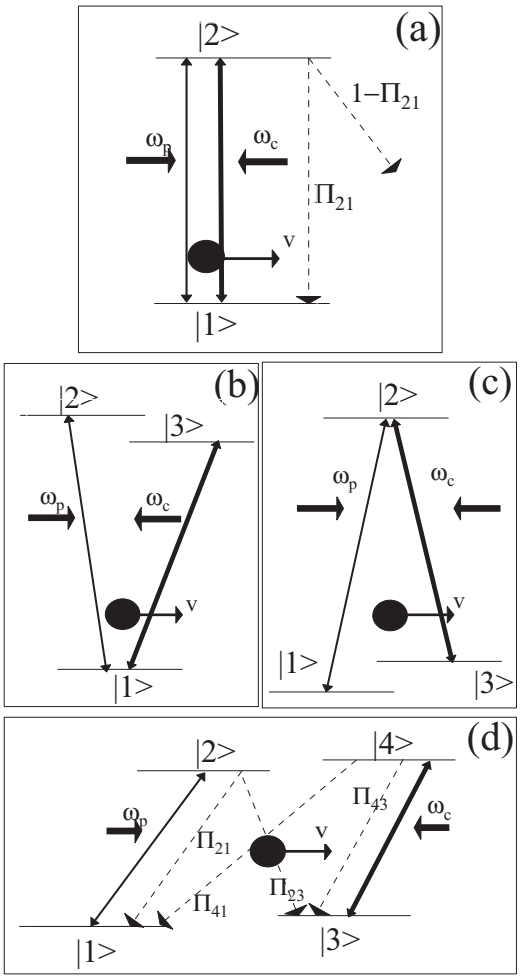


FIG. 1. Level schemes for the sub-Doppler saturation spectroscopy: (a) two-level scheme, (b) three-level V scheme, (c) three-level Λ scheme, and (d) N four-level scheme. Strong control laser at angular frequency $\omega_c$ and weak probe laser at angular frequency $\omega_p$ traveling in opposite directions excite the atomic levels. In panels (a) and (d) the spontaneous emission coupling between levels $i \rightarrow j$ is described by the branching ratios $\Pi_{ij}$.

In saturation spectroscopy atoms moving in random directions are irradiated by two laser beams, control and probe of frequencies $\omega_c$ and $\omega_p$, with intensities $I_c$ and $I_p$, respectively. The strong control laser modifies the atomic population, and the weak probe laser monitors those modifications. The saturation spectroscopy eliminates Doppler broadening by using control and probe beams traveling in opposite directions. Because of Doppler shift the atoms having an axial velocity $v$ in the laboratory frame experience the control and probe laser beams shifted in frequency to $\omega_p - kv$ and $\omega_c + kv$, with $k$ being the laser wave number, as schematized in Fig. 1 for different atomic level schemes. Only atoms moving in a narrow velocity range along the optical axis interact simultaneously with control and probe lasers.

To analyze our results we solve the optical Bloch equations in the presence of the control laser and use that solution to calculate the absorption of the probe laser. An important ingredient is the openness of the transitions driven by the two lasers. For the simplest case of a two-level transition like in

Fig. 1(a) that character is described by the branching ratio $\Pi_{21}$ from the upper $|2\rangle$ level to the lower one and by the complement $1-\Pi_{21}$ towards other levels.

### A. Steady-state regime

Under the control laser excitation, by eliminating the atomic coherences within the optical Bloch equations like in Refs. [19,24], for a given atomic velocity $v$ the $\rho_{11}$ and $\rho_{22}$ populations within the $|1\rangle$ and $|2\rangle$ levels, respectively, of Fig. 1(a) are given by

$$\frac{\partial}{\partial t}\rho_{11} = \Gamma_c(\rho_{22}-\rho_{11}) + \Gamma\Pi_{21}\rho_{22} - \gamma\left(\rho_{11}-\rho_{11}^0\right),$$
$$\frac{\partial}{\partial t}\rho_{22} = -\Gamma_c(\rho_{22}-\rho_{11}) - \Gamma\rho_{22}, \tag{2}$$

with $\Gamma$ being the excited state spontaneous decay rate, and $\gamma$ being the rate at which atoms are produced in the ground state $|1\rangle$. The steady-state occupation $\rho_{11}^0(v)$ is given by

$$\rho_{11}^0(v) = W(v) = \frac{1}{\sqrt{\pi}u}e^{-\left(\frac{kv}{\Delta_D}\right)^2}. \tag{3}$$

$W(v)$ is the Gaussian atomic velocity distribution, with $\Delta_D = ku$ being the Doppler width, $u=(2k_BT/M)^{1/2}$ being the most probable velocity, where $T$ is the gas temperature, $k_B$ is the Boltzmann constant, and $M$ is the atomic mass. $\Gamma_c$ is the control laser pumping rate [24]

$$\Gamma_c = \left(\Omega_{1-2}^c\right)^2\frac{\Gamma}{\Gamma^2+4\Delta_c^2} = f_{1-2}\frac{I_c}{2I_{\rm sat}}\frac{\Gamma}{1+4\Delta_c^2/\Gamma^2}, \tag{4}$$

where $\Omega_{1-2}^c$ is the laser Rabi frequency and $\Delta_c$ is the laser detuning for the driven transition. The control pumping rate has been rewritten on the basis of the $f_{1-2}$ line strength and of the $I_{\rm sat}$ saturation intensity for the $B=0$ cycling transition reported in Ref. [25].

The $I_p$ laser probes the $|1\rangle-|2\rangle$ population difference perturbed by the control laser. The steady-state population difference derived from Eqs. (2) determines the probe laser absorption coefficient and the amplitude of the TLS saturated absorption signal. For a weak probe laser, the absorption is proportional to the $I_p$ probe intensity. For coupling and probe resonant frequencies $\omega_c=\omega_p=\omega_{21}$ and a given $I_p$ laser intensity we characterize the absorption amplitude through the following dimensionless $f^{\rm TLS}$ parameter:

$$f^{\rm TLS} = -f_{1-2}\frac{I_c}{I_c+I_{\rm op}}, \tag{5}$$

depending on the $f_{1-2}$ strength of the absorbing transition. The $I_{\rm op}$ optical pumping saturation intensity in Ref. [19], or depletion saturation intensity in Ref. [24], is given by

$$I_{\rm op} = \frac{I_{\rm sat}}{f_{1-2}}\frac{1+\frac{\gamma}{\Gamma}}{1+\frac{\Gamma(1-\Pi_{21})}{2\gamma}}. \tag{6}$$

For our present target of comparing different TLS strengths, the $f^{\rm TLS}$ parameter does not include the $W(0)=(\sqrt{\pi}u)^{-1}$ fraction of absorbing atoms at zero velocity. The negative sign within Eq. (5) implies that the atomic absorption is decreased by the control laser saturation. Most experimental observations are performed at $I_c \gg I_{\rm op}$ and therefore $|f^{\rm TLS}| \approx f_{1-2}$.

### B. Transient regime

Within the optical pumping process a key role is played by the $\tau_{\rm op}$ optical pumping time [24]:

$$\tau_{\rm op} = \frac{1+\Gamma_c/\Gamma}{\Gamma_c(1-\Pi_{21})}. \tag{7}$$

If $\tau_{\rm op}$ is comparable or larger than $1/\gamma$, the above steady-state approach is not valid. In Ref. [24] the saturated absorption signal is obtained by imposing $\gamma=0$ within Eqs. (2) and integrating from 0 to $1/\gamma$ their time-dependent solution. The final result for the $f$ parameter within this transient regime is

$$f_{\rm tran}^{\rm TLS} = -f_{1-2}\left[1-\frac{I_{\rm sat}}{f_{1-2}I_c(1-\Pi_{21})}(1-e^{-\tau_{\rm op}\gamma})\right], \tag{8}$$

Notice that both the optical pumping saturation intensity and the pumping time play a key role in transitions with $\Pi_{21}$ close to 1.

## III. CROSSOVER SATURATION SIGNALS

Crossover (CO) saturation spectroscopy has been investigated by a large number of authors in a variety of level schemes. Our attention is concentrated on the VTL and N configurations represented in Figs. 1(b) and 1(d). For the VTL configuration the control and probe lasers act on two transitions, $|1\rangle\rightarrow|2\rangle$ and $|1\rangle\rightarrow|4\rangle$, respectively, sharing the lower state $|1\rangle$. For the N four-level scheme the control and the probe act on two separate transitions $|1\rangle\rightarrow|2\rangle$ and $|3\rangle\rightarrow|4\rangle$ and a coupling between the laser actions is produced by spontaneous emissions processes $|2\rangle\rightarrow|3\rangle$ and/or $|4\rangle\rightarrow|3\rangle$ with branching ratios $\Pi_{23}$ and $\Pi_{41}$. Both processes were identified for the first time in Refs. [8,9]. CO signals produced by the $\Lambda$ saturation scheme of Fig. 1(c) are not observed in our $\pi\pi$ and $\sigma\sigma$ polarizations because for our magnetic fields the ground-state Zeeman splittings are larger than the Doppler width and no atoms are available for $\Lambda$ schemes.

### A. V-scheme crossover

The $f^{\rm VTL}$ signal amplitude of the VTL signal is derived by including an additional upper level to the TLS analysis of Sec. II. Extending that analysis to the probe laser acting on the $|1\rangle\rightarrow|2\rangle$ transition and the control laser acting on the $|1\rangle\rightarrow|3\rangle$ transition, we obtain for the resonant steady state the $f^{\rm VTL}$ amplitude:

$$f^{\rm VTL} = -\frac{W(v)}{W(0)}f_{12}\frac{\left[1+\frac{\Gamma}{\gamma}(1-\Pi_{31})\right]f_{13}I_c}{\left(1+\frac{\gamma}{\Gamma}\right)I_{\rm sat}+\left(1+\frac{\Gamma}{\gamma}\frac{1-\Pi_{31}}{2}\right)f_{13}I_c}, \tag{9}$$

with the Gaussian $W(v)$ probability calculated at the atomic velocity $v$ given by

$$v = \frac{1}{2k}[(\omega_{31}-\omega_c)-(\omega_{21}-\omega_p)] \tag{10}$$

and the resonance condition

$$\omega_c+\omega_p = \omega_{21}+\omega_{31}. \tag{11}$$

The $W(v)/W(0)$ fraction in Eq. (9) describes the strength reduction owing to the reduced number of absorbing atoms at velocity $v$. It is included in order to compare the $f^{\rm TLS}$

parameters to the corresponding ones for the multilevel systems. The minus sign indicates that the saturated VTL produces a decreased absorption. Due to the investigated regime $I_p \ll I_c$ our analysis neglects the contribution of the coherence between the upper levels [26], because the laser intensity $I_p$ is very small as compared to $I_c$. As pointed out in Refs. [9,10], within a three-level system the role of control and probe lasers may be reversed. Therefore two different velocity classes, given by Eq. (10) and its opposite, determine the total VTL signal amplitude.

### B. N and double-N crossovers

In a single N-scheme the probe laser acts on the $|1\rangle \rightarrow |2\rangle$ transition and the control laser acts on the $|3\rangle \rightarrow |4\rangle$ one with one-way coupling $\Pi_{41} \neq 0$, i.e., $\Pi_{23} = 0$ [see Fig. 1(d)]. The resonant $f^N$ CO amplitude is given by

$$f^N = \frac{W(v)}{W(0)} f_{12} \frac{\Pi_{41} f_{34} I_c}{\frac{\gamma}{\Gamma}\left(1+\frac{\gamma}{\Gamma}\right) I_{\rm sat} + \left(\frac{1-\Pi_{43}}{2} + \frac{\gamma}{\Gamma}\right) f_{34} I_c}, \quad (12)$$

with $W(v)$ corresponding to the resonant atomic velocity

$$v = \frac{1}{2k}[(\omega_{43} - \omega_c) - (\omega_{21} - \omega_p)] \quad (13)$$

and the resonance condition

$$\omega_c + \omega_p = \omega_{21} + \omega_{43}. \quad (14)$$

Again the $W(v)/W(0)$ fraction describes the strength reduction due to the reduced number of absorbing atoms at velocity $v$. The positive sign indicates that the N saturation signal corresponds to an increased absorption. Within the single N scheme the role of the control and probe lasers cannot be reversed and only one velocity class contributes to the signal.

The double-N COs are associated with a four-level structure where spontaneous emission decays are present in both directions, i.e., both $\Pi_{23}$ and $\Pi_{41}$ are different from zero. Thus the overall level structure is equivalent to two separate N schemes, (1-2-3-4) and (3-4-1-2), where the roles of the control and probe lasers are reversed. Two different velocity classes at $v$ given by Eq. (13) and at its opposite contribute to the absorption signals. The double-N amplitude is obtained by summing up the $f^N$ amplitudes of each N configuration. The medium-high magnetic field spectrum of rubidium atoms contains some very strong double-N COs where a complete symmetry exists between the levels. The two transitions driven by the control and probe lasers have comparable transition strengths, i.e., $\Pi_{21} \approx \Pi_{43}$, and that applies also to the decay rates, i.e., $\Pi_{23} \approx 1 - \Pi_{21} \approx \Pi_{41} \approx 1 - \Pi_{43}$.

## IV. APPARATUS

The experiments are performed with a commercial grating-feedback laser diode (Toptica Photonics, DLX110) operating in the Littrow configuration. The 780-nm laser diode, stabilized in temperature, has a typical 1-MHz free-running linewidth and an output power up to 500 mW, but after optical fiber cleaning only a power less than 5 mW is used for each of the saturated absorption setups listed in the following. Part of the laser emission is sent into a homemade FabryPerot interferometer (FPI), with a 200-MHz free-spectral-range and 250 finesse, whose transmission peaks provide a frequency reference for the measurements of rubidium spectral features. A commercial wavemeter was used for very precise frequency measurements.

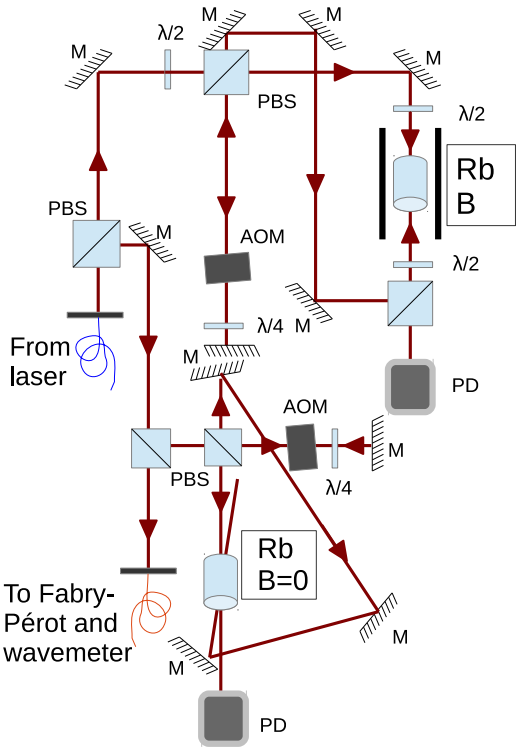


FIG. 2. (Color online) Schematic diagram of the apparatus having two separated saturated absorption setups, in a $B \approx 0$ Rb cell and in one at medium-high $B$ field, and using as reference a Fabry-Pérot reference cavity or a wavemeter. Component symbols: AOM acousto-optic modulator, PBS polarizing beam splitter, PD photodiode, $\lambda/2$ and $\lambda/4$ phaseplates, M mirror.

The laser power is injected into two saturated absorption spectroscopy setups, shown in Fig. 2, one containing a rubidium cell placed in the laboratory background magnetic field and the second one containing a cell placed within permanent magnets. The rubidium homemade vapor cells contain $^{85}$Rb and $^{87}$Rb in natural abundance. The control beam is frequency modulated by passing through an AOM in double passage, and lock-in detection at the 60-kHz modulation frequency is applied to the probe's transmitted light. The diameter of the probe laser beam, around 3 mm leading to $\gamma = 1\times10^5$ s$^{-1}$, is smaller than that of the control laser. The control and probe laser propagations within the cell are perpendicular to the magnetic field direction.

Saturated absorption spectra on the $D_2$ transition are recorded by scanning the laser frequency, and examples are given in Figs. 3 and 4(a). The absorption lines appear with a derivative line shape because of the lock-in detection. The FPI output port allows us to monitor the laser power over the frequency scan and to correct the spectrum intensity for variations of the $I_p$ intensity. For each absorption line we determine the relative amplitude $S_{\rm meas}$ defined as the integrated intensity of the saturated absorption. Because the

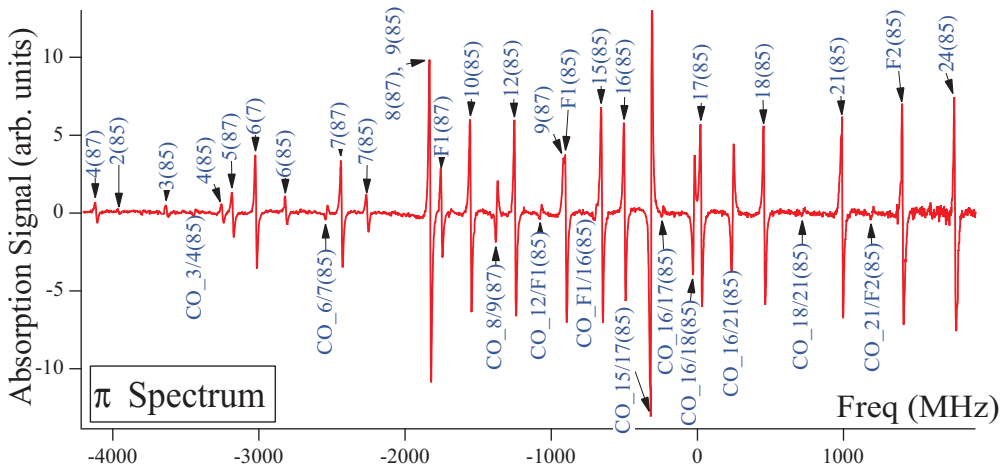


FIG. 3. (Color online) Derivative of the rubidium sub-Doppler absorption spectrum vs the laser frequency for an applied $B = 0.126$ T field and $\pi$ polarization of both control and probe laser beams. The spectrum covers a 6-GHz-wide spectral range, limited by laser instabilities on the high-frequency side. The zero frequency is the center of gravity of the $B = 0$ $^{85}$Rb spectra. The transitions are numbered following their increasing frequency position at $B = 0$, with the isotope number in parentheses at the end. For the zero-field forbidden transitions, F1 and F2, of $^{85}$Rb and the F1 one of $^{87}$Rb appearing within the spectrum, the quantum numbers are reported within the text. All the appearing COs are produced by N schemes with the an increased absorption, and the −316-MHz strongest one is produced by a double-N level scheme.

absorption derivatives are recorded [see Figs. 3 and 4(a)], $S_{\rm meas}$ is obtained by fitting the measured signal to the derivative of an absorption Lorentzian line shape. In the case of strong absorption lines we introduce into $S_{\rm meas}$ a correction for the sample optical thickness. We take the $B = 0$ $^{87}$Rb $|F_g = 2, m_g = 2\rangle \rightarrow |F_g = 3, m_g = 3\rangle$ saturated signal as a reference signal with $S_{\rm meas} = 1$. Because the operations of removing the magnet assembly and replacing it with a $B = 0$ cell are not systematically performed, the $S_{\rm meas}$ values have an estimated 10% indetermination.

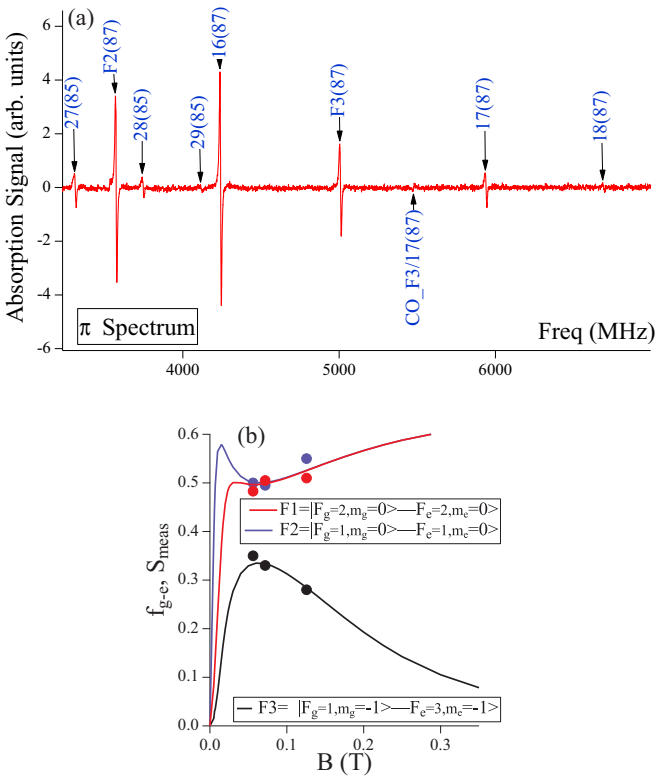


FIG. 4. (Color online) (a) Spectrum for the same conditions as in Fig. 2 with two, F2 and F3, $^{87}$Rb zero-field forbidden lines. (b) Line strength $f_{g-e}$ vs magnetic field $B$ for the $^{87}$Rb F1–F3 lines with their $B = 0$ quantum numbers reported in the inset. The dots denote the $S_{\rm meas}$ experimental observations normalized to the black line value at 0.072 T. There is a 10% indetermination associated with the experimental values.

An eight-pole Halbach-like [27] magnetic field configuration, similar to those described in Refs. [28–30], provides a uniform field within the laser-atom interaction region. It is created by assembling in a cylindrical configuration several small NdFeB permanent magnets, with a 1.08-T remnant magnetic field. Magnet assemblies with different radial dimensions are fabricated to produce the magnetic fields explored in this work. Numerical investigations like Ref. [28] indicate that our assembly is able to produce fields up to few Tesla with an homogeneity around $10^{-3}$ T within the atomic volume illuminated by the laser, 3 mm in diameter and 20 mm in length. After a rough estimation of the magnetic field measured with a Hall probe, we derive the value of the magnetic field acting on the atoms by comparing the position of all the observed saturation absorption lines to a simulated spectrum based on the Rb parameters reported in Ref. [25]. The magnetic field indeterminacy is setup by the inhomogeneous broadening of the absorption lines. The laboratory background field, estimated from the reference apparatus, is $<10^{-4}$ T.

## V. SPECTRA

For the investigations reported here with magnetic fields in the range between 0.05 and 0.13 T, the hyperfine coupled basis $|F_g, m_g\rangle_g$ is perfectly valid for the atomic ground state, but it is not exact for the excited state, where the magnetic interaction is larger than the hyperfine coupling. However following the seminal work by Tremblay *et al.* [11] that explored the rubidium absorption in a similar magnetic field

range, we adopt the hyperfine coupled basis also for the excited state and denote the transitions as $|F_g,m_g\rangle \rightarrow |F_e,m_e\rangle$.

Saturated absorption spectra recorded with $\pi$ polarizations of both control and probe lasers for the applied magnetic field $B = 0.126$ T are shown in Figs. 3 and 4(a). These spectra present a quite large number of lines, and the complexity increases when the $\sigma/\sigma$ polarization configuration is explored. We have not studied the $\pi/\sigma$ configuration where the spectrum is even more crowded. The spectra contain lines with opposite signs. All lines produced by saturated absorption with control and probe lasers acting on the same two-level system, as in Fig. 1(a), have the same sign. They are numbered in the upper part of the spectra, with the isotope indication in parentheses at the end. The reported numbers denote their position in the spectra at increasing frequency. Because of the different Zeeman splittings in the ground and excited states, the $B = 0$ sequence does not match always the frequency order of the large magnetic fields of the present investigation.

Few two-level lines denoted as F (forbidden) are present in both spectra. They are forbidden at $B = 0$ because of the optical dipole selection rules. At the intermediate magnetic field they become allowed by the magnetic field mixing of the hyperfine eigenstates, as recently investigated for rubidium in Ref. [15] and for caesium in Ref. [16]. Within the magnetic field range of the present investigation, the forbidden lines acquire a large probability, as evidenced by the those appearing in the $B = 0.126$ T $\pi$ spectra of Figs. 3 and 4(a). The theoretical and measured intensities of the F1–F3 lines of $^{87}$Rb, with their quantum numbers, are reported in Fig. 4(b) as a function of the magnetic field. The forbidden lines for the $^{85}$Rb isotope appearing within the spectrum of Fig. 3 are identified as $\mathrm{F1(85)} = |3,0\rangle_g \rightarrow |3,0\rangle_e$ and $\mathrm{F2(85)} = |2,0\rangle_g \rightarrow |2,0\rangle_e$. In Ref. [15] few forbidden lines were investigated at a slightly lower field, ≈0.02 T. At lower fields the spectrum becomes much too crowded to measure precisely the lines strengths.

The remaining spectra lines, labeled as $\mathrm{CO}_{xx}$ in the bottom, are associated with the CO level schemes. The CO features are determined by the two optical transitions, and their labels are inserted into each CO label. The CO laser resonance condition is the median of the participating transitions, as easily verified. That condition is very useful in deriving the quantum numbers of the participating levels. All CO signals of both reported spectra are produced by the four-level configuration of Fig. 1(c). They correspond to an increased absorption and therefore have a sign opposite to that of the two-level signals. The spectrum of Fig. 3 is characterized by a very strong CO at −316-MHz frequency produced by a very symmetric double-N scheme, $\Pi_{21} \approx \Pi_{43} \approx 0.6$ and $\Pi_{23} \approx \Pi_{41} \approx 0.3$.

COs associated with the V scheme of Fig. 1(b) produce absorption signals with the same sign as the two-level ones. However at $B = 0.126$ T very few were detected because for most existing V schemes the frequency separation between the upper levels is much larger than the ≈500-MHz Doppler width, and very few atoms have the resonant velocity required by Eq. (10). V-scheme COs were detected in the spectra recorded at lower magnetic fields. For instance, a 0.072-T-wide scanning $\sigma/\sigma$ spectrum contained 82 absorption lines, with 27 N and 1 VTL COs.

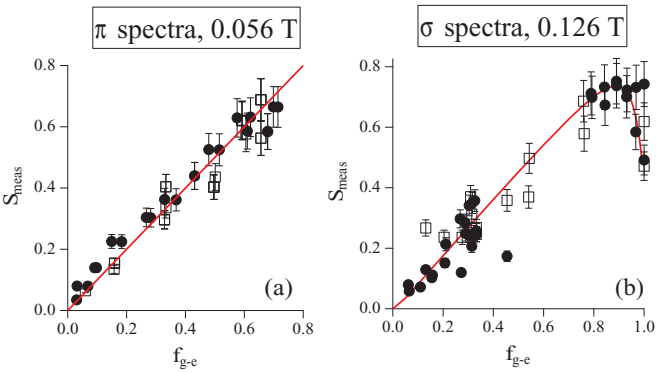


FIG. 5. (Color online) Comparison between the $S_{\mathrm{meas}}$ intensities of TLS saturation signals (data points) and the $f^{\mathrm{TLS}}$ theoretical predictions (continuous red lines) vs the $f_{g-e}$ of the absorption line, all dimensionless. Closed circles for $^{85}$Rb data and open squares for $^{87}$Rb ones. (a) $\pi/\pi$ polarization signals at 0.056 T. (b) $\sigma/\sigma$ polarization signals at 0.126 T. Theoretical predictions are derived from Eq. (5) in panel (a) and from Eq. (8) in panel (b) with $I_c = 2I_{\mathrm{sat}}$ and $\gamma = 1.10^5$ s$^{-1}$.

## VI. LINE STRENGTHS

Figure 5(a) reports the $S_{\mathrm{meas}}$ measurements of TLS on a $\pi/\pi$ spectrum at 0.056 T, for a control laser intensity of $I_c = 2I_{\mathrm{sat}}$, equivalent to $I_c \rightarrow \infty$ in Eq. (5). Therefore $|f^{\mathrm{TLS}}| \approx f_{g-e}$ and the linear dependence of $S_{\mathrm{meas}}$ on $f_{g-e}$ predicted by that equation is confirmed. Figure 5(b) reports the TLS measurements on a $\sigma/\sigma$ spectrum at 0.126 T at the same control laser intensity in the presence of transitions with a large variety of $f_{g-e}$ values, and several of them close to 1. Notice that for those values the linear dependence prediction is not satisfied. Instead a dependence of $S_{\mathrm{meas}}$ on $f_{g-e}$ with an intermediate maximum is predicted by the treatments of both Refs. [19] and [24], including the role of the transient regime. Figure 5(b) shows the good theory-experiment agreement using Eq. (8). Notice that the deviation from the linear regime appears only for $f_{g-e} \geqslant 0.8$ and therefore the data of Fig. 5(a) are well fitted by the linear dependence. Only for optical transitions with a large excitation probability does the slow optical pumping process towards other states modify the linear dependence predicted by the steady state. For some $\sigma/\sigma$ polarization data, theory-experiment discrepancies are observed, and we attribute them to the presence of unidentified CO signals superimposed on the identified ones.

Figure 6 reports similar comparisons for the CO signals, in panel (a) for a $\pi/\pi$ spectrum at 0.056 T and in panel (b) for a $\sigma/\sigma$ spectrum at 0.072 T. Following our sign convention, we plot $S_{\mathrm{meas}}$ measured for the N signals with a negative sign in order to distinguish them from the VTL signals. The $f^{\mathrm{VTL}}$ theoretical predictions for the VTL positive values are from Eq. (9), and the $f^N$ ones for the N negative values are from Eq. (12). The red lines represent theoretical predictions based on the TLS linear dependence reported in Fig. 5 confirming the correct absolute scale of $S_{\mathrm{meas}}$. Among the larger number of COs observed at the lower magnetic field, several data deviate from the theoretical predictions, and once again we attribute this to the presence of unidentified COs.

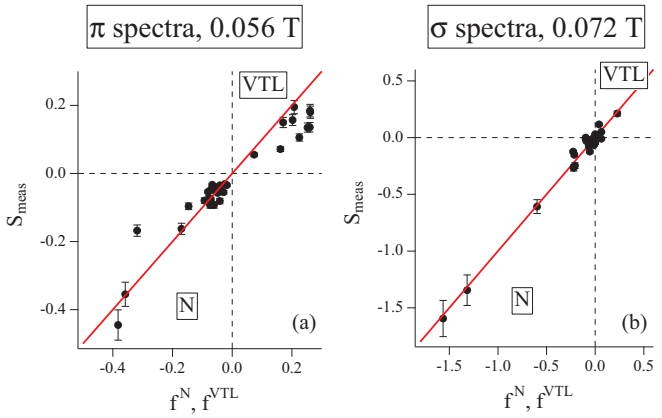


FIG. 6. (Color online) $S_{\rm meas}$ intensities of VTL and N saturation signals (data points) vs $f^{\rm VTL}$ or $f^N$, all dimensionless. Positive values correspond to VTL signals, described by Eq. (9), and negative values correspond to N signals, described by Eq. (12). (a) Signals at 0.056 T in a $\pi/\pi$ spectrum. (b) Signals at 0.072 T in a $\sigma/\sigma$ spectrum. The red lines report theoretical predictions based on the TLS linear dependence of Fig. 5(a).

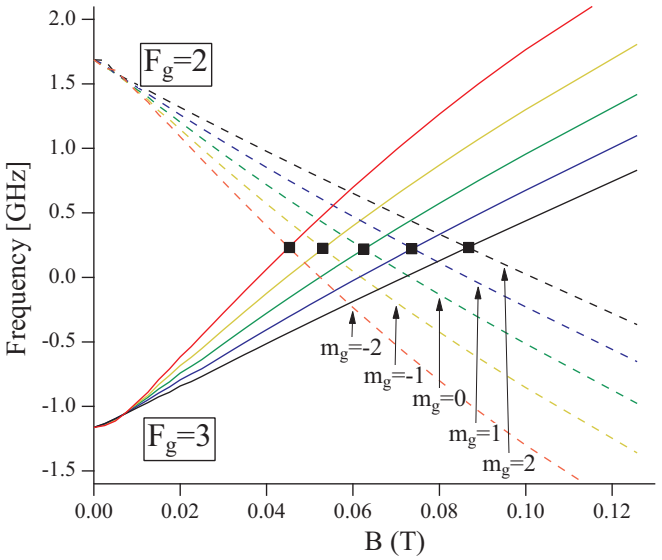


FIG. 7. (Color online) Frequencies vs $B$ magnetic field for $^{85}$Rb optical transition couples producing strong double-N COs in $\sigma/\sigma$ driving. Magic field values are denoted by the black squares. Continuous lines are for $\sigma^+$ transitions from $|F_g=3,m_g\rangle_g$ states to $|F_e,m_e\rangle_e$ states, and dashed lines are for $\sigma^-$ transitions from $|F_g=2,m_g\rangle_g$ states. In black $|3,2\rangle_g \rightarrow |4,3\rangle_e$ (first from bottom), $|2,2\rangle_g \rightarrow |1,1\rangle_e$ (first from top); in blue $|3,1\rangle_g \rightarrow |4,2\rangle_e$ (second from bottom), $|2,1\rangle_g \rightarrow |1,0\rangle_e$ (second from top); in green $|3,0\rangle_g \rightarrow |4,1\rangle_e$ (third from bottom), $|2,0\rangle_g \rightarrow |1,-1\rangle_e$ (third from top); in yellow $|3,-1\rangle_g \rightarrow |4,0\rangle_e$ (fourth from bottom), $|2,-1\rangle_g \rightarrow |2,-2\rangle_e$ (fourth from top); in red $|3,-2\rangle_g \rightarrow |4,-1\rangle_e$ (fifth from bottom), $|2,-2\rangle_g \rightarrow |3,-3\rangle_e$ (fifth from top). The zero frequency is the center of gravity of the $B=0$ $^{85}$Rb spectra. At $B=0$ the transitions are separated by the 3-GHz ground-state hyperfine splitting.

All the N CO signals with $|f^N|>0.3$ are produced by double-N schemes, and within the $\sigma$ spectra intensities larger than the $f_{g-e}=1$ value associated with the $B=0$ cycling transition of $^{87}$Rb are fairly common [see those two present in Fig. 6(b)]. Most COs of the $\sigma/\sigma$ spectra are associated with a common level configuration, with ground states within the scheme of Fig. 1(d) such as $|1\rangle=|F_g=I-1/2,m_g\rangle$ and $|3\rangle=|F_g=I+1/2,m_g\rangle$, where $I$ is the nuclear spin quantum number, 3/2 and 5/2 for the two Rb isotopes, respectively. Within the explored magnetic range, those ground states are coupled to excited states by the $\sigma^+/\sigma^-$ $B=0$ allowed transition with $f_{g-e}$ line strengths larger than 0.4. In addition, all the $|2\rangle$ and $|4\rangle$ excited states have very similar branching decay rates, i.e., $\Pi_{21}\approx\Pi_{43}$ between 0.6 and 0.4, and $\Pi_{23}\approx\Pi_{41}$ between 0.6 and 0.4. Therefore the N signals created by exchanging the action of the control and probe lasers on each N scheme have comparable intensity, contributing to a total strong intensity. Examples of those transitions are listed within the caption of Fig. 6. The $\pi/\pi$ configuration COs are produced by the Fig. 1(d) scheme with $|1\rangle=|F_g,m_g\rangle$ and $|3\rangle=|F_g,m_g\pm1\rangle$, the $\Pi_{23}$ and $\Pi_{41}$ decay channels being associated with the $\sigma$ transitions. These COs have intensities smaller than those of $\sigma/\sigma$ excitations because the laser-driven $\pi$ transitions are weaker than the laser-driven $\sigma$ transitions.

For all the cases reported in this work the laser-driven $|1\rangle\rightarrow|2\rangle$ and $|3\rangle\rightarrow|4\rangle$ transitions have different frequencies, and the atomic velocity compensates for that difference. For the case of $\omega_c=\omega_p$ the resonant atomic velocity condition of Eq. (13) requires $|\omega_{21}-\omega_{43}|\leqslant 2ku$, i.e., twice the Doppler width of 500 MHz.

## VII. PERSPECTIVE AND CONCLUSIONS

Our observed double-N COs are produced by two different velocity classes as it appears from Eq. (13) imposing $\omega_{21}\neq\omega_{43}$. However by properly tuning the magnetic field it is possible to identify magic values where the condition $\omega_{21}=\omega_{43}$ is satisfied. Then, for $\omega_p=\omega_c$ at the magic magnetic fields a single atomic zero velocity class interacts simultaneously with the control and probe lasers driving each N scheme of the double-N signals. This is shown in Fig. 7 for the case of $\sigma/\sigma$ driving of the coupling and probe transitions and for level schemes with $|1\rangle=|F_g=I-1/2,m_g\rangle$ and $|3\rangle=|F_g=I+1/2,m_g\rangle$. Examples of the frequency dependence on the $B$ magnetic field for those coupled transitions forming the double-N signals are reported there. The magic field values are denoted by black squares. Other combinations with the same ground states and different excited states also produce strong double-N COs. In $^{87}$Rb owing to the larger ground-state hyperfine splitting similar double-N schemes are realized at magnetic fields in the 0.1–0.2 T range. At the magic magnetic field values the absorbing atoms experience a *push-pull* evolution between the four levels, similar to the push-pull evolution in double-Λ-driven systems [31,32]. It will be interesting to investigate if the transient regime of the absorption signals could present new additional features. In addition at the magic magnetic field values of Fig. 7 applying two separate laser radiations driving the $|1\rangle\rightarrow|4\rangle$ and $|3\rangle\rightarrow|2\rangle$ transitions a double-Λ scheme is realized where two separate atomic transitions are driven by the same laser. For such a magic field configuration the processes of electromagnetically induced transparency and slow light will be enhanced. The magic field values for $^{85}$Rb are within the

range explored within the present investigation. It may be difficult to assemble a permanent magnet generating exactly the magic value. Instead that value may be reached more easily by tuning the field with additional Helmoltz coils.

We have performed a sub-Doppler spectroscopic analysis of the Rb isotope absorption in magnetic fields within the 0.05–0.13 T range. We have identified a large number of absorbing transitions. In addition the spectra present a large number of COs produced by three-level V-scheme and four-level N configurations. No $\Lambda$-scheme CO is detected, but several of them should appear within the mixed $\pi/\sigma$ laser scheme, even if their intensity will be not very large because most transitions are open. Our recorded spectra present very strong saturated absorption signals produced by double-N configurations where two different atomic velocity classes contribute to the absorption.

The intensities are analyzed through a simple model, providing a complete picture for both two-level and many-level signals. The agreement between theory and experiment may be improved by developing a model of the transient regime for the COs and applying the Doppler analysis to both the two-level resonances and the COs.

In our experimental observations the laser-induced population transfers among the levels of N four-level schemes are incoherently produced by spontaneous emission processes. However, all the explored incoherent N schemes can be transformed into coherent ones by applying an additional resonant laser radiation. Therefore all alkali-metal atoms immersed in medium-high magnetic fields have a large number of strong and easily accessible coherent double-N coherent configurations.

As a quite straightforward application of the present scheme within the medium-high field regime and based on permanent magnets that split the alkali-metal absorption lines, a strong reference line can be produced at any frequency close to the $B = 0$ ones (within a 20-GHz interval) by properly choosing the applied magnetic field. A well-designed magnet assembly reducing the present field inhomogeneity will produce narrow absorption lines good enough for a simple, but precise and stable, reference setup.

## ACKNOWLEDGMENTS

Thisresearch has been partially supported through NEXT (Grant No. ANR-10-LABX-0037) in the framework of the "Programme des Investissements d'Avenir." S.S. acknowledges financial support from Université Franco Italienne, and E.A. acknowledges financial support from the Chair d'Excellence Pierre de Fermat of the Conseil Regional Midi-Pyrenées. The authors acknowledge the valuable technical assistance of Nicola Puccini in realizing the magnetic assembly; the preparation by Nicolas Bruyant of the software recording simultaneously data from absorption, a FPI, and a wavemeter; and the support of Remy Battesti and Mathilde Fouché. E.A. is very grateful to Renaud Mathevet for sharing his atomic physics knowledge.

[1] M. Fleischhauer, A. Imamoglu, and J. P. Marangos, Electromagnetically induced transparency: Optics in coherent media, Rev. Mod. Phys. **77**, 633 (2005).

[2] S. E. Harris and Y. Yamamoto, Photon Switching by Quantum Interference, Phys. Rev. Lett. **81**, 3611 (1998).

[3] M. Yan, E. G. Rickey, and Y. Zhu, Observation of absorptive photon switching by quantum interference, Phys. Rev. A **64**, 041801(R) (2001).

[4] D. A. Braje, V. Balic, S. Goda, G. Y. Yin, and S. E. Harris, Frequency Mixing using Electromagnetically Induced Transparency in Cold Atoms, Phys. Rev. Lett. **93**, 183601 (2004).

[5] H. Kang, G. Hernandez, and Y. Zhu, Resonant four-wave mixing with slow light, Phys. Rev. A **70**, 011801(R) (2004).

[6] Y.-F. Chen, Z.-H. Tsai, Y.-C. Liu, and I. A. Yu, Low-light-level photon switching by quantum interference, Opt. Lett. **30**, 3207 (2005).

[7] T. Y. Abi-Salloum, B. Henry, J. P. Davis, and F. A. Narducci, Resonances and excitation pathways in four-level N-scheme atomic systems, Phys. Rev. A **82**, 013834 (2010).

[8] Ph. Cahuzac and R. Damaschini, Pressure effects in a saturated-absorption experiment on the 587.5 nm helium line, Opt. Commun. **20**, 111 (1977).

[9] S. Nakayama, G. W. Series, and W. Gawlik, Zeeman effect in the polarization spectroscopy of Na, Opt. Commun. **34**, 382 (1980).

[10] S. Nakayama, Optical pumping effects in high resolution laser spectroscopy, Phys. Scr. **T70**, 64 (1997).

[11] P. Tremblay, A. Michaud, M. Levesque, S. Theriault, M. Breton, J. Beaubien, and N. Cyr, Absorption profiles of alkali-metal $D$ lines in the presence of a static magnetic field, Phys. Rev. A **42**, 2766 (1990).

[12] M. Ummal Momeen, G. Rangarajan, and P. C. Deshmukh, Variations of intensity in Rb $D_2$ line at weak/intermediate fields, J. Phys. B **40**, 3163 (2007).

[13] G. Skolnik, N. Vujicic, and T. Ban, Optical pumping of the Zeeman components in the rubidium vapor, Opt. Commun. **282**, 1326 (2009).

[14] B. A. Olsen, B. Patton, Y.-Y. Jau, and W. Happer, Optical pumping and spectroscopy of Cs vapor at high magnetic field, Phys. Rev. A **84**, 063410 (2011).

[15] G. Hakhumyan, C. Leroy, R. Mirzoyan, Y. Pashayan-Leroy, and D. Sarkisyan, Study of forbidden atomic transitions on $D_2$ line using Rb nano-cell placed in external magnetic field, Eur. Phys. J. D **66**, 199 (2012).

[16] A. Sargsyan, A. Tonoyan, G. Hakhumyan, A. Papoyan, E. Mariotti, and D. Sarkisyan, Giant modification of atomic transition probabilities induced by a magnetic field: Forbidden transitions become predominant, Laser Phys. Lett. **11**, 055701 (2014).

[17] T. W. Hänsch, Nonlinear high resolution spectroscopy of atoms and molecules, in *Nonlinear Spectroscopy*, *Proceedings of the International School of Physics "E. Fermi", Course LXIV*, edited by N. Bloembergen (North-Holland, Amsterdam, 1977), p. 17.

[18] H. K. Holt, Theory of Laser Saturation Spectroscopy, Phys. Rev. Lett. **29**, 1138 (1972).

[19] P. G. Pappas, M. M. Burns, D. D. Hinshelwood, M. S. Feld, and D. E. Murnick, Saturation spectroscopy with laser optical pumping in atomic barium, Phys. Rev. A **21**, 1955 (1980).

[20] H. D. Do, M. S. Heo, G. Moon, H. R. Noh, and W. Jhe, Analytic calculation of the lineshapes in polarization spectroscopy of rubidium, Opt. Commun. **281**, 4042 (2008).

[21] G. Moon and H.-R. Noh, A comparison of the dependence of saturated absorption signals on pump beam diameter and intensity, J. Opt. Soc. Am. B **25**, 2101 (2008).

[22] H.-R. Noh, G. Moon, and W. Jhe, Discrimination of the effects of saturation and optical pumping in velocity-dependent pump-probe spectroscopy of rubidium: A simple analytical study, Phys. Rev. A **82**, 062517 (2010).

[23] D. A. Smith and I. G. Hughes, The role of hyperfine pumping in multilevel systems exhibiting saturated absorption, Am. J. Phys. **72**, 631 (2004).

[24] I. Sydoryk, N. N. Bezuglov, I. I. Beterov, K. Miculis, E. Saks, A. Janovs, P. Spels, and A. Ekers, Broadening and intensity redistribution in the Na($3p$) hyperfine excitation spectra due to optical pumping in the weak excitation limit, Phys. Rev. A **77**, 042511 (2008).

[25] D. Steck, Alkali D line data, available at http://steck.us/alkalidata/

[26] E. G. Saprykin, A. A. Chernenko, and A. M. Shalagin, On the shape of cross resonances in counterpropagating wave spectroscopy, Opt. Spectrosc. **113**, 530 (2012).

[27] K. Halbach, Design of permanent multipole magnets with oriented rare earth cobalt material, Nucl. Instrum. Methods **169**, 1 (1980).

[28] P. Cheiney, O. Carraz, D. Bartoszek-Bober, S. Faure, F. Vermersch, C. M. Fabre, G. L. Gattobigio, T. Lahaye, D. Guéry-Odelin, and R. Mathevet, A Zeeman slower design with permanent magnets in a Halbach conguration, Rev. Sci. Instrum. **82**, 063115 (2011).

[29] E. Danieli, J. Perlo, B. Blümich, and F. Casanova, Highly Stable and Finely Tuned Magnetic Fields Generated by Permanent Magnet Assemblies, Phys. Rev. Lett. **110**, 180801 (2013).

[30] D. Haa, J. Paulsenb, N. Sunc, Y.-Q. Songb, and D. Hama, Scalable NMR spectroscopy with semiconductor chips, Proc. Natl. Acad. Sci. USA **111**, 11955 (2014).

[31] Y.-Y. Jau, E. Miron, A. B. Post, N. N. Kuzma, and W. Happer, Push-pull Optical Pumping of Pure Superposition States, Phys. Rev. Lett. **93**, 160802 (2004).

[32] T. Zanon, S. Guerandel, E. de Clercq, D. Holleville, N. Dimarcq, and A. Clairon, High Contrast Ramsey Fringes with Coherent-Population-Trapping Pulses in a Double Lambda Atomic System, Phys. Rev. Lett. **94**, 193002 (2005).